

ClueTracer: Question-to-Vision Clue Tracing for Training-Free Hallucination Suppression in Multimodal Reasoning

Gongli Xi^{1*}, Kun Wang^{2*}, Zeming Gao¹, Huahui Yi³, Haolang Lu¹, Ye Tian¹, and Wendong Wang¹

¹ Beijing University of Posts and Telecommunications, Beijing, China

{yetian,kevinxgl,zemenggao,1h1_2507,wdwang}@bupt.edu.cn

² Nanyang Technological University, Singapore

wang.kun@ntu.edu.sg

³ West China Biomedical Big Data Center, West China Hospital, SCU

Abstract. Large multimodal reasoning models solve challenging visual problems via explicit long-chain inference: they gather visual clues from images and decode clues into textual tokens. Yet this capability also increases hallucinations, where the model generates content that is not supported by the input image or the question. To understand this failure mode, we identify *reasoning drift*: during clue gathering, the model over-focuses on question-irrelevant entities, diluting focus on task-relevant cues and gradually decoupling the reasoning trace from visual grounding. As a consequence, many inference-time localization or intervention methods developed for non-reasoning models fail to pinpoint the true clues in reasoning settings. Motivated by these insights, we introduce CLUERECALL, a metric for assessing visual clue retrieval, and present CLUETRACER, a training-free, parameter-free, and architecture-agnostic plugin for hallucination suppression. CLUETRACER starts from the question and traces how key clues propagate along the model’s reasoning pathway (question \rightarrow outputs \rightarrow visual tokens), thereby localizing task-relevant patches while suppressing spurious attention to irrelevant regions. Remarkably, **without any additional training**, CLUETRACER improves all **reasoning** architectures (including R1-OneVision, Ocean-R1, MM-Eureka, *etc.*) by **1.21 \times** on reasoning benchmarks. When transferred to **non-reasoning** settings, it yields a **1.14 \times** gain.

1 Introduction

In recent years, large multimodal language models (MLLMs) have undergone a paradigm shift from simple image description to unified cross-modal reasoning, giving rise to Multimodal Large Reasoning Models (MLRMs) [26,15]. These models establish multi-step logical inference chains across visual, textual, and auditory inputs, enabling systematic problem-solving and decision-making in

* These authors contributed equally.

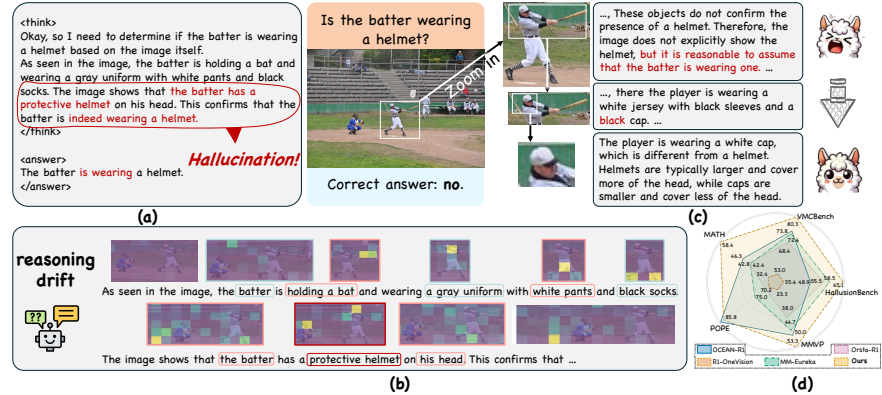


Fig. 1. (a) Example outputs from a reasoning model; hallucinated content is highlighted in red. (b) Reasoning drift in a multimodal reasoning model, where attention during inference is allocated to task-irrelevant regions. (c) An intuitive illustration: by progressively zooming in on task-critical regions, hallucinations (in red) diminish and the answers become correct. (d) Radar-chart comparisons among different reasoning models; CLUETRACER is training-free and architecture-agnostic.

complex, real-world scenarios [61,50]. To endow them with “thinking” capabilities, practitioners apply supervised fine-tuning or reinforcement learning to a pre-trained multimodal backbone, thereby strengthening their inferential strategies and generalization on demanding tasks [48,53,13].

Despite these advantages, stronger reasoning often comes with exacerbated *hallucination*—the generation of content incongruent with the input or factually incorrect [29,63,4,24]. While MLRMs inherit hallucination tendencies from MLLMs, the issue can be amplified in the reasoning setting: the generation pipeline remains language-dominant and produces lengthy deliberations, encouraging over-reliance on linguistic priors and under-utilization of visual clues [17,6]. This modal imbalance weakens visual grounding and increases the likelihood of fabricating non-existent objects or causal explanations not supported by the image [46,10].

A related challenge is what we term *reasoning drift* (*i.e.*, attentional diffusion toward task-irrelevant details). Because MLRMs typically marshal numerous “clues” en route to an answer [52,45], many of which are extraneous to the question, attention can scatter away from visually decisive regions. For example, as illustrated in Fig. 1 (a) and (b), when asked “*Is the batter wearing a helmet?*,” the model first enumerate attire attributes (*e.g.*, white pants, black socks), which exceeds the scope of the question and dilutes focus on the helmet. An intuitive example in Fig. 1 (c) further shows that progressively constraining the attended image region to key areas guides the model’s reasoning back to visually decisive cues, thereby reducing hallucination and recovering the correct answer. This

suggests that the model’s capacity is not the bottleneck; rather, ungrounded and cluttered clue collection can derail an otherwise solvable reasoning process.

In practice, localizing task-critical visual clues at inference time faces two coupled difficulties—(i) **long-horizon output control** and (ii) **limited generalization beyond object-centric tasks**—because many existing mitigation strategies embed implicit assumptions about where **clues** come from. One implicit assumption is *token-role-agnostic*: visual grounding can be improved without conditioning on which tokens the model generates, so global inference-time biasing (e.g., contrastive decoding [20,19,16], logit steering [1,22], or attention reallocation [18,37,5]) can be applied to keep the model looking at the image. While effective for short-form responses, such methods introduce a persistent bias that compounds over long reasoning traces and can overlook the decisive clues that appear in intermediate reasoning steps [62]. Another implicit assumption is *task-agnostic*: the task merely triggers a search, and all necessary clues can be harvested from the image—motivating pipelines that elicit richer image descriptions or captions as priors before answering [11,52]. However, in complex reasoning problems (e.g., math or logic) [41], the question itself supplies indispensable constraints and intermediate clues; richer image description alone cannot provide the missing structure. Together, these mismatches explain why prior inference-time methods that work for non-reasoning MLLMs can fail to reliably isolate the *decisive* clues under long-chain multimodal reasoning.

To address these mismatches, we introduce CLUERECALL, a layer-wise visual-grounding metric that measures each layer’s ability to retrieve question-relevant clues, and propose CLUETRACER, a training-free, parameter-free plugin that localizes task-critical **visual clues** by explicitly **tracing** how they propagate across the model’s three interacting streams: the query stream, the output stream, and the visual stream. Instead of assuming that key clues can be derived from any single stream in isolation (e.g., image-only priors or output-agnostic control), CLUETRACER starts from the question to identify its decisive constraints, then uses the model’s own intermediate outputs as an explicit bridge to determine which generated tokens actually operationalize those constraints, and finally traces these key tokens back to the minimal set of supporting visual regions. This clue-flow tracing (**query** → **output** → **vision**) directly couples the task with the image, isolating only the evidence required by the question, and stabilizes long-chain reasoning by re-anchoring the generation to these traced clues.

Our contributions are as follows:

- **(CLUERECALL) Average Recall by Attention.** We introduce CLUERECALL as a model-internal metric to probe visual perception in MLLMs. Using this metric, we observe that in 7B (28-layer) architectures the perception signal peaks at layers **18–24**, reaching $\sim 50\%$ CLUERECALL.
- **(CLUETRACER) Hallucination suppression in reasoning architectures.** We identify the *reasoning drift* phenomenon in MLRs and propose CLUETRACER, a training-free mechanism that routes native attention from **question** → **output** → **visual** to accurately localize task-relevant evidence. On reasoning-oriented hallucination benchmarks, CLUETRACER yields an average

1.25 \times improvement on **HallusionBench** and **1.17 \times** on **VMCBench**, while markedly reducing reasoning drift and strengthening perceptual focus.

- **Transferability to non-reasoning MLLMs.** CLUETRACER is *architecture-agnostic* and transfers to non-reasoning settings, lifting some models (*e.g.*, LLaVA-1.6, R1-OneVision) from near chance to the GPT-4V range. On non-reasoning benchmarks, CLUETRACER achieves an **average** accuracy improvement of **+8.7** percentage points.

2 Related Work

Multimodal Large Reasoning Models (MLRMs). Early works extended chain-of-thought (CoT) reasoning to vision-language models through supervised fine-tuning and reinforcement learning (RL), with methods like Marco-01 integrating search and reflection strategies [61]. Subsequent approaches enhanced stepwise reasoning via self-refinement [54] and long-chain data scaling [48], while VLMs adopted CoT supervision for visual reasoning [26,35,50]. Preference-based RL alignment emerged to reduce factual errors using human feedback [53], closed-loop optimization [57], and reasoning trace comparisons [7]. The GRPO paradigm introduced by DeepSeek-R1 established rule-based reward optimization as standard practice [13,28,55,15,42,32]. Two dominant approaches exist: **1) Two-stage SFT+RL pipelines** (*e.g.*, R1-OneVision, Reason-RFT) [49,34,56], and **2) Direct large-scale RL training** (“R1-Zero”) yielding emergent reasoning [33,44]. Recent innovations include unified frameworks for joint reasoning/perception [31] and RL-enhanced generative reasoning [8].

Hallucination in MLRMs. Extended reasoning chains exacerbate visual hallucinations as models increasingly rely on language priors over visual evidence [4,24]. Inference-time mitigation methods largely fall into two lines: **(i) token-role-agnostic grounding** that applies step-invariant interventions—*e.g.*, contrastive decoding [20,19,16], logit steering [1,22], or attention control/reallocation [18,37,5,51]—which can accumulate bias over long traces and miss decisive intermediate evidence [62]; and **(ii) task-agnostic priors** that prepend generic descriptions/captions before answering [11,52], yet often fail to capture question-conditional constraints in complex reasoning tasks (*e.g.*, multimodal math) [41]. As multimodal tasks diversify and reasoning becomes longer-horizon, recent progress increasingly emphasizes training-time alignment and reasoning-centric resources [6,17,58,10,64,46,40]. Yet existing work still lacks a step-aware, question-conditional inference-time mechanism that reliably isolates *decisive* visual clues throughout long-chain multimodal reasoning.

3 Preliminaries

Multimodal Large Reasoning Models (MLRMs). We consider decoder-style multimodal systems that connect a pretrained visual encoder to a language model via a projector. The visual encoder and projector map the image into a sequence of visual tokens \mathbf{X}_v . The input \mathbf{X}_c is the concatenation of system tokens \mathbf{X}_s , visual

tokens \mathbf{X}_v , and question tokens \mathbf{X}_q , i.e., $\mathbf{X}_c = [\mathbf{X}_s, \mathbf{X}_v, \mathbf{X}_q]$, with lengths N_s , N_v , and N_q , and total length $N_c = N_s + N_v + N_q$. At each decoding step t , the model samples a token y_t from a conditional distribution $p(y_t | \mathbf{X}_c, \mathbf{y}_{<t})$, where $\mathbf{y}_{<t} = \{y_i\}_{i=1}^{t-1}$. Reasoning-oriented MLLMs yield explicit reasoning traces in response to instructions [27,60]: in typical settings, the model prints its internal “thinking” between `<think>` `</think>` tags, followed by the final answer.

Attention Mechanism in MLRMs. Given an MLRM with a Transformer [38] decoder of L layers and an output sequence of length T , we denote by $\mathbf{A}_{t,l} \in [0, 1]^{N_c+t-1}$ the attention distribution at layer l and decoding step t over the *available context tokens*, i.e., the multimodal prefix \mathbf{X}_c together with previously generated tokens $\mathbf{y}_{<t}$. Concretely, letting $\mathbf{X}^{(t)} = [\mathbf{X}_c; \mathbf{y}_{<t}]$ and $N^{(t)} = |\mathbf{X}^{(t)}| = N_c + t - 1$, we write

$$\mathbf{A}_{t,l,:} = \text{softmax} \left(\frac{Q_t^{(l)} K_{(t)}^{(l)\top}}{\sqrt{d_k}} \right), \quad \sum_{i=1}^{N^{(t)}} A_{t,l,i} = 1,$$

where $K_{(t)}^{(l)}$ are the keys formed from all available tokens in the step- t context $\mathbf{X}^{(t)}$. We refer to \mathbf{A} as the *attention tensor*, which records, for every decoding step and layer, the normalized distribution over the context tokens, enabling token-level attribution and layer-wise aggregation.

4 Motivations

We conduct three targeted study to understand the thinking process of MLRMs and distill three observations (***Obs1–Obs3***) that directly motivate our design in CLUETRACER. Each observation is backed by a minimal, controlled study and quantitative evidence.

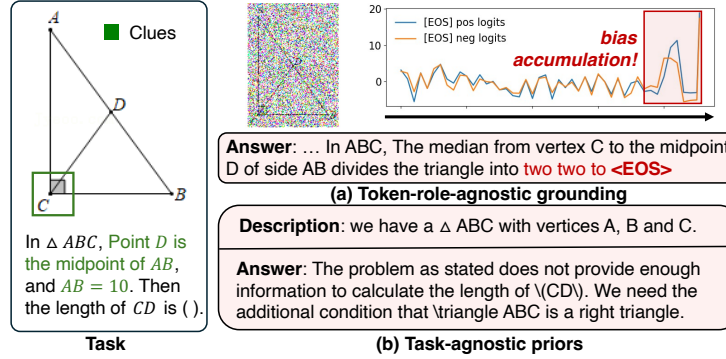


Fig. 2. Failure modes of prior mitigation: (a) bias accumulation and (b) clue neglect.

Obs 1: Bias accumulation and clue neglect in prior inference-time methods

As shown in Fig. 2, directly steering output logits or attention weights can encourage an MLRM to rely more on visual signals, but in long-chain reasoning it may induce *bias accumulation*, which can prematurely trigger the `<eos>` token. For example, in VCD, constructing a noisy negative counterpart and applying step-wise contrast can cause decoding to drift after a certain step, eventually making the `<eos>` logits dominant. Meanwhile, task-agnostic prior methods (e.g., generic captioning or global image-description prompting) still risk overlooking task-critical clues that are present in the image.

Obs 2: Task-relevant clues are traceable across streams via the output

Data context. Using paired *(question, object annotation)* data, we can automatically recover a *clue propagation path* without any extra labeling. Concretely, POPE provides yes/no questions instantiated from the template “Is there a/an *{object}* in the image?” and MSCOCO supplies the aligned object categories and bounding boxes for the same images [21,23]. We treat the annotated object region as the ground-truth visual clue, then (i) locate the output steps where the model explicitly mentions the queried object, and (ii) read out the model’s attention at the selected layer over three domains: query tokens, output tokens, and visual tokens. This yields a fully automatic, token-level trace of how question constraints are expressed in the generated outputs and how those outputs in turn connect to the image evidence. Additional details are deferred to Appendix D [47].

The resulting traces reveal a consistent mediation pattern: when an output step is strongly aligned with the question’s key query clues, the same step exhibits concentrated support on a small set of visual tokens covering the decisive region—even if surrounding steps attend broadly or drift to irrelevant content. In other words, the task-relevant visual clue is often *not* directly separable from the query or the image alone; it becomes identifiable when conditioning on *which outputs operationalize the query*.

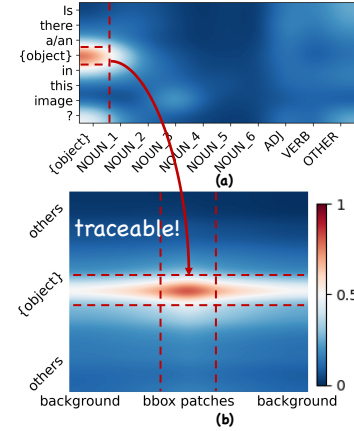


Fig. 3. (a) Question to Output Heat-map. (b) Visual to Output Heatmap. The dashed outline denotes expected attention region, consistent with the heatmap.

Obs3: Key question tokens show larger **attention variance** along the output dimension.

Extending ***Obs2***, key question tokens exhibit localized attention peaks along the output axis; consequently their attention traces show larger variance than non-key tokens, providing an efficient, training-free signal for key-token detection.

These observations provide a pathway to suppress hallucinations in MLRMs: using the output as a conduit from the input question to the visual tokens. Concretely, we first identify key question tokens, then select question-relevant output tokens, and finally locate the visual tokens most tightly linked to the question. The procedure is applied at inference time, requiring **no additional training or manual annotations**; because it is performed before the final input is fed to the MLRM, it is **architecture-agnostic and transferable**.

5 Method

In this paper, we present CLUETRACER, an inference-time approach that leverages an MLRM’s long reasoning chain to isolate visual clues critical for answering the question. We first introduce CLUERECALL, a layer-wise visual-grounding metric that identifies the decoder layer where clue retrieval is most reliable (Sec. 5.1). Building on this, CLUETRACER traces key clues across the model’s three streams, progressively localizing pivotal patch tokens via question \rightarrow output \rightarrow vision computations (Sec. 5.2). Finally, we describe how the traced patches are organized into reusable clue regions for downstream reasoning (Sec. 5.3). As shown in Fig. 4, CLUETRACER uses stream-aware clue tracing to pinpoint the minimal visual support required for problem solving, thereby re-grounding generation and mitigating hallucinations.

5.1 CLUERECALL: Assessing Visual Clue Retrieval

Perception is a prerequisite for reliable reasoning. The goal of CLUERECALL is to assess, for each layer of an MLRM, how well its visual attention captures question-relevant visual clues. A single image typically contains multiple dense visual clusters, but only a subset is truly informative for answering a given question (*e.g.*, when asked “Is the batter wearing a helmet?”, the decisive evidence should lie on the batter rather than the catcher). As a precursor to our method, CLUERECALL runs an automatic pipeline that measures how much attention each layer allocates to task-critical regions in three steps:

Query construction. For each image I , we obtain its set of bounding boxes and category labels cat from either annotations (*e.g.*, COCO [23]) or a segmentation model (*e.g.*, Mask R-CNN [14]). For each category, we instantiate a query using the fixed template $q_{\text{cat}} = \text{“Is there a/an } \{\text{cat}\} \text{ in this image?”}$, and tokenize it into question tokens $\mathbf{X}_{q_{\text{cat}}}$.

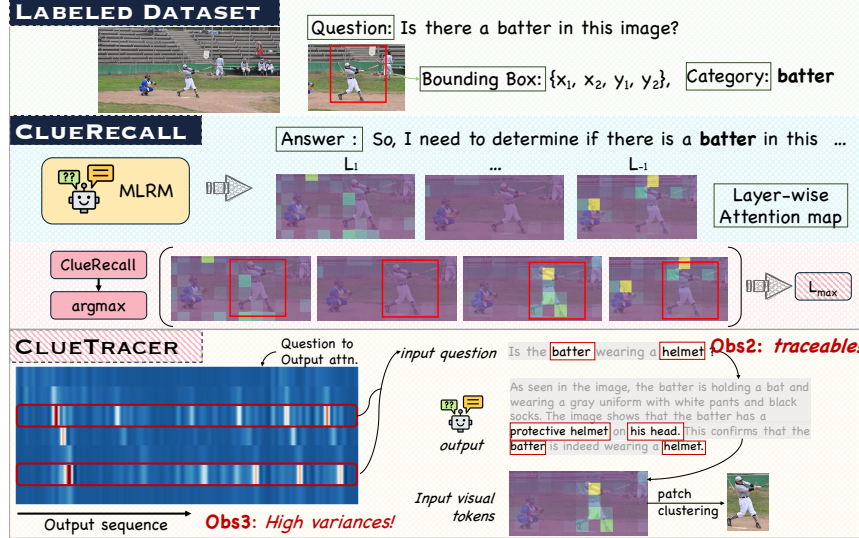


Fig. 4. Overview of our methods. **Top:** labeled data used by CLUERECALL, the `bbox` and `cat` can either come from COCO annotations or a lightweight model, enabling our pipeline to extend to arbitrary datasets. **Middle:** computing layer-wise CLUERECALL and selecting the layer L_{\max} with the strongest visual clue retrieval. **Bottom:** CLUETRACER follow the question \rightarrow output \rightarrow visual attention pathway to progressively localize task-relevant visual regions. Best viewed in color.

Query-aligned regions. For each (I, q_{cat}) pair, we treat the corresponding bounding box of category `cat` as the question-relevant clues. We encode I into visual tokens \mathbf{X}_v with the visual encoder and projector, and map the bounding box to its covered visual-token indices, denoted by $\mathbf{X}_{\text{bbox}} \subseteq \mathbf{X}_v$.

CLUERECALL. Collecting all such perception-labeled instances yields a set $\mathcal{X}_{\text{perc}} = \{(\mathbf{X}_{q_{\text{cat}}}, \mathbf{X}_v, \mathbf{X}_{\text{bbox}}, \text{cat})\}$. For each item in $\mathcal{X}_{\text{perc}}$, we prepend the system prompt \mathbf{X}_s to form the complete input $\mathbf{X}_c = [\mathbf{X}_s, \mathbf{X}_v, \mathbf{X}_{q_{\text{cat}}}]$, feed it into the reasoning model \mathcal{R} , and obtain output tokens $\{y_1, \dots, y_T\}$ and the attention tensor $\mathbf{A} \in [0, 1]^{T \times L \times N_v}$. Let \mathcal{V} denote the visual-token indices within \mathbf{X}_c , and let $\mathbf{A}_{t,l,\mathcal{V}} \in [0, 1]^{N_v}$ be the restriction of $\mathbf{A}_{t,l}$ to these visual indices. We evaluate each layer l by how well its visual attention, at the exact output steps where the category token is mentioned, retrieves the ground-truth region \mathbf{X}_{bbox} . For each layer $l \in \{1, \dots, L\}$, we define

$$\text{CLUERECALL}(l) = \frac{1}{|\mathcal{X}_{\text{perc}}|} \sum_{\mathbf{X}_c \in \mathcal{X}_{\text{perc}}} \frac{|\text{TopK}_{|\mathbf{X}_{\text{bbox}}|}(\sum_{t: y_t = \text{cat}} \mathbf{A}_{t,l,\mathcal{V}}) \cap \mathbf{X}_{\text{bbox}}|}{|\mathbf{X}_{\text{bbox}}|} \quad (1)$$

which directly measures a layer’s ability to retrieve object-aligned patches when the object is explicitly mentioned in the model’s output. Accordingly, we set $L_{\max} \triangleq \arg \max_{l \in \{1, \dots, L\}} \text{CLUERECALL}(l)$ and use L_{\max} as the reference layer for all subsequent clue-tracing computations.

5.2 CLUETRACER: Task-Critical Token Identification

Building on CLUERECALL, we have identified the layer with the strongest *clue retrieval*, denoted by L_{\max} . In CLUETRACER, we move to a more general setting: we ask *how to recover task-critical visual regions when neither bounding-box annotations nor fixed question templates are available?* To this end, we leverage the observations in Sec. 4 and use the pathway from question \rightarrow output \rightarrow visual tokens to progressively mine task-relevant clues.

Key query tokens via output-axis variability. In **Obs 3**, we find that when the model’s output is tightly aligned with the question, the decoder repeatedly allocates attention to a small set of key query tokens. As a result, the attention trajectory of these key tokens along the output axis becomes highly non-uniform, exhibiting larger variance than that of non-key tokens. We therefore collect query-side attention at layer L_{\max} across the entire output axis and retain query tokens whose standardized variability is high. Let $\mathcal{Q} \subseteq \{1, \dots, N_c\}$ denote the index set of query tokens within \mathbf{X}_c . For each query index $n_q \in \mathcal{Q}$ and each decoding step $t \in \{1, \dots, T\}$, we write

$$A_{t,n_q} = A_{t,L_{\max},n_q}, \quad \mathbf{a}_{n_q} = (A_{1,n_q}, \dots, A_{T,n_q}) \in \mathbb{R}^T, \quad (2)$$

where \mathbf{a}_{n_q} is the attention trajectory of the n_q -th query token x_{n_q} over the output steps. We compute the variance $\text{Var}(\mathbf{a}_{n_q})$ for each $n_q \in \mathcal{Q}$, and select key query tokens as

$$\mathcal{X}_q^* = \{ x_{n_q} \in \mathbf{X}_q : \text{zscore}(\text{Var}(\mathbf{a}_{n_q})) \geq \tau_q \}, \quad (3)$$

where $\text{zscore}(\cdot)$ denotes the standard score obtained by subtracting the mean and dividing by the standard deviation [39]. The indices in \mathcal{X}_q^* correspond to query tokens whose attention trajectories exhibit high output-axis variability and are thus treated as key query clues.

Tracing visual clues via Query-Output-Vision propagation. Having identified the key query clues \mathcal{X}_q^* , we seek the *task-supporting* visual evidence: a subset of visual tokens $\mathcal{X}_v^* \subset \mathbf{X}_v$ that best *grounds* these query constraints and thus suffices to solve the task. We formalize this as selecting \mathcal{X}_v^* to maximize the query-conditioned support $P(\mathcal{X}_v^* | \mathcal{X}_q^*)$. However, under autoregressive (causally-masked) decoding, this dependency is not directly observable and is effectively mediated by the intermediate outputs, motivating a posterior signal. To bridge this, CLUETRACER leverages the model’s intermediate reasoning chain $\mathbf{y}_{1:T}$ as

latent variables. We formulate the relevance of a visual token x_v to the query constraints as a probabilistic trace, marginalizing over the output steps:

$$P(x_v | \mathcal{X}_q^*) = \sum_{t=1}^T \underbrace{P(x_v | y_t)}_{\text{Visual Grounding}} \cdot \underbrace{P(y_t | \mathcal{X}_q^*)}_{\text{Query Alignment}}. \quad (4)$$

In this formulation, $P(y_t | \mathcal{X}_q^*)$ represents how strongly step t aligns with the query constraints, and $P(x_v | y_t)$ represents the visual support required by that step. In practice, we instantiate this probabilistic flow using the attention map at layer L_{\max} , which CLUERECALL identifies as the most reliable layer for *clue retrieval*. We define the *Trace Score* $\mathcal{T}_{\mathcal{R}}(x_v)$ under the reasoning model \mathcal{R} by instantiating the probabilities with normalized attention weights:

$$P(x_v | \mathcal{X}_q^*) \propto \mathcal{T}_{\mathcal{R}}(x_v) = \sum_{t=1}^T \underbrace{\left(\sum_{x_{n_q} \in \mathcal{X}_q^*} A_{t, L_{\max}, n_q} \right)}_{\text{Query Alignment}} \cdot \underbrace{A_{t, L_{\max}, v}}_{\text{Visual Grounding}}. \quad (5)$$

Eq. (5) effectively creates a continuous flow of importance from the query, through the reasoning bottleneck, to the image. High scores are assigned to visual tokens that are repeatedly attended to by reasoning steps that are themselves highly sensitive to the question. Finally, to suppress background noise, we apply a statistical filtering function $\psi(\cdot)$ (implemented via z -score normalization [39]) to select the final task-critical set:

$$\mathcal{X}_v^* = \{x_v \in \mathbf{X}_v \mid \psi(\mathcal{T}(x_v)) \geq \tau_v\}. \quad (6)$$

This traced set \mathcal{X}_v^* represents the minimal visual clues sufficient to support the query constraints, derived not from heuristics but from the model’s dynamics.

5.3 Evidence-Region Construction and Inference-Time Use

Organization. Starting from the selected visual tokens \mathcal{X}_v^* , we map each token $x_v^* \in \mathcal{X}_v^*$ to its image-plane center $\phi(x_v^*) \in \mathbb{N}^2$, cluster the point set $\{\phi(x_v^*)\}_{x_v^* \in \mathcal{X}_v^*}$ with DBSCAN [9] to obtain clusters $\{C_r\}_{r=1}^R$, and enclose each cluster by an axis-aligned rectangle $R_r = \text{BBox}(C_r)$. The resulting region set $\mathcal{R} = \{R_1, \dots, R_R\}$ defines crops of the original image. This construction preserves the model’s native rectangular interface while consolidating fragmented evidence into a small number of spatially coherent *visual clues*.

Input modes. We use these crops in two complementary ways. *Offline*: precompute and cache \mathcal{R} for repeated evaluation or families of similar images. *Online*: a two-stage inference pipeline—**Stage 1** derives \mathcal{R} from the model; **Stage 2** re-invokes the model on $(I; \mathcal{R})$ to refine reasoning with focused evidence.

Table 1. Comparison on reasoning-oriented hallucination benchmarks with and without CLUETRACER. qAcc, fAcc, hAcc, and aAcc denote, respectively, the accuracy *per question pair*, *per figure*, *on hard questions*, and the *overall average*. Case studies are provided in Appendix C.4 [47].

Model	HallusionBench (Accuracy %)				VMCBench (Accuracy %)					Average Δ Acc
	qAcc	fAcc	hAcc	aAcc	Gen.	Reason.	OCR	Math	Doc&Chart	
R1-OneVision	8.57	12.43	31.86	35.43	56.64	45.14	65.39	32.44	52.35	52.99
+CLUETRACER	24.18	40.17	54.42	58.90	76.11	61.81	89.97	51.21	78.88	73.91
Ocean-R1	19.34	27.76	40.00	48.89	77.74	61.69	88.91	46.25	76.58	73.75
+CLUETRACER	30.11	43.35	54.88	63.51	83.51	66.99	97.19	53.36	85.11	80.32
MM-Eureka	23.07	31.50	49.30	58.46	76.31	58.79	90.46	42.44	76.21	72.44
+CLUETRACER	33.41	47.11	56.98	65.10	83.56	67.26	94.05	58.38	85.93	80.31
Orsta-R1	21.76	28.61	45.81	55.45	71.55	55.62	85.06	42.82	72.60	68.39
+CLUETRACER	27.91	36.71	53.49	60.05	81.52	64.21	94.41	51.11	84.63	78.39

6 Experiments

In this section, we conduct experiments to address the following research questions:

- **RQ1.** How well does CLUETRACER reduce hallucinations and improve accuracy across diverse reasoning architectures? Which layer best reflects the model’s understanding?
- **RQ2.** During generation, can CLUETRACER mitigate reasoning drift exhibited in Fig. 1, maintaining alignment between the question focus and produced content?
- **RQ3.** How do results change when key settings varied, and specifically, does CLUETRACER’s output-mediated patch selection outperform baselines designed for non-reasoning MLLMs?
- **RQ4.** Does CLUETRACER transfer to non-reasoning MLLMs (e.g., LLaVA, Qwen), demonstrating robust, architecture-agnostic generalization?

6.1 Experimental Setup

We begin with a concise overview of models, datasets, and evaluation metrics; full implementation and protocol details are deferred to the Appendix Section B [47].

Models. CLUETRACER is compatible with existing hallucination-mitigation schemes for MLRs. Accordingly, we apply it to several reasoning models—R1-OneVision [49], Ocean-R1 [33], Orsta-R1 [31], and MM-Eureka [32]—to assess generality. To test transferability, we also port CLUETRACER to *non-reasoning* MLLMs, including LLaVA-1.6-Mistral [25] and Qwen2.5-VL [3].

Datasets & Evaluation Metrics. We evaluate on four widely used hallucination benchmarks, grouped as follows: *reasoning-oriented*: 1) **VMCBench** [59], a unified multiple-choice questions drawn from 20 VQA datasets, e.g., *Math-Vision* [41], *ScienceQA* [30], and 2) **HallusionBench** [12] benchmarks image-context reasoning where language hallucinations and visual illusions are

Table 2. Per-layer CLUERECALL (left) and benchmark accuracy on POPE/MMVP with and without CLUETRACER (right). Higher is better.

Model	CLUERECALL per Layer (%)						POPE (%)		MMVP (%)	
	0	6	12	18	24	27	w/o CT	w/ CT	w/o CT	w/ CT
R1-OneVision	30.78%	33.68%	43.11%	50.60%	47.28%	44.11%	70.22%	76.97%	23.33%	46.00%
Ocean-R1	31.05%	32.64%	48.56%	53.79%	50.92%	49.23%	86.77%	85.77%	47.33%	50.00%
MM-Eureka	29.30%	30.57%	45.45%	51.06%	51.38%	48.11%	75.00%	81.38%	44.67%	50.00%
ORSTA-R1	31.14%	32.38%	47.55%	51.66%	55.32%	50.56%	71.36%	82.98%	38.00%	53.33%

entangled; and *perception-oriented*: **3) POPE** [21] and **4) MMVP** [36]. We follow each dataset’s official evaluation protocol.

6.2 Performance with CLUETRACER on Reasoning Models (RQ1)

To assess hallucination in *reasoning* models, we evaluate each model *before* and *after* applying CLUETRACER on hallucination benchmarks; the results are reported in Table 1 and Table 2, Additional results on **other variants** and **larger models** are provided in Appendix C [47]. We can draw the following findings:

Finding 1: Consistent gains across models and datasets. CLUETRACER improves *all* reasoning models across the four hallucination benchmark. Specifically, on the reasoning-oriented hallucination datasets—**HallusionBench** and **VMCBench**—CLUETRACER achieves a **maximum** accuracy gain of **22.20%** and an **average** accuracy gain of **11.84%**.

Finding 2: Models with different training architectures exhibit similar perceptual capacity. From Table 2, the CLUERECALL curves for all models peak at **layer 18 or layer 24** and follow a rise–then–fall pattern. On the perception-oriented hallucination benchmarks—**POPE** and **MMVP**—CLUETRACER delivers an **average** absolute gain of **8.73%**.

6.3 Hallucination Analysis (RQ2)

To further verify the hallucination-suppression ability of CLUETRACER, we compute two key indicators on the POPE dataset: (1) *{object} visual attention*, i.e., the attention mass that falls inside the *{object}* bounding box; and (2) *{object} text proportion*, i.e., the fraction of noun tokens in the model output that correspond to *{object}*, we also present examples where the model reduces reasoning drift and strengthens perceptual focus, as shown in Fig. 5. Our key findings are as follows:

Finding 3: CLUETRACER mitigates reasoning drift. As shown in Fig. 5 (a), after models are equipped with CLUETRACER, the *{object} text proportion* in the generated text **increases** markedly across all models. Fig. 5 (b) provide two illustrative cases. *Without* CLUETRACER, the model offers exploratory descriptions of irrelevant regions while **overlooking** the truly discriminative area; *with* CLUETRACER, it **directly focuses** on the region that needs to be judged. In Fig. 5 (b-2), for example, the baseline over-attends to non-key areas (*desk* →

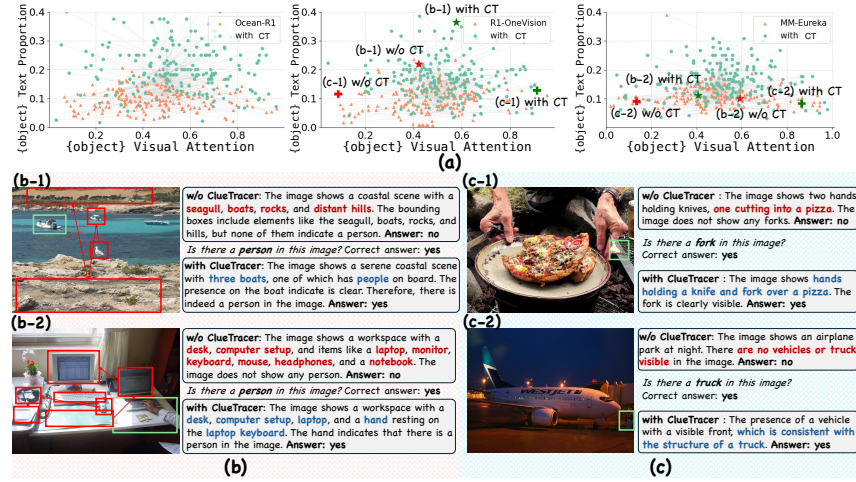


Fig. 5. (a) Comparative scatter plot of attention allocation versus output mentions for task-relevant objects; (b) case study showing that CLUETRACER reduces reasoning drift; (c) case study showing that CLUETRACER enhances fine-grained perceptual sensitivity.

computer setup \rightarrow *laptop* \rightarrow *monitor* \rightarrow *keyboard* \rightarrow *mouse* \rightarrow *headphones* \rightarrow *notebook*), thereby **missing** the hand in the bottom-right corner.

Finding 4: CLUETRACER reduces perceptual hallucination. As shown in Fig. 5, CLUETRACER allocates **higher attention to key regions**, enabling the model to attend to areas that were hard to perceive. In Fig. 5 (c-2), for instance, CLUETRACER surfaces a faint truck silhouette that humans also found subtle; prior to applying CLUETRACER, all reasoning models answered “no.”

6.4 Component Studies (RQ3)

As discussed in previous sections, CLUETRACER effectively identifies task-relevant visual evidence. In this section, we examine the *module sensitivity* of CLUETRACER and explain why analogous approaches developed for *non-reasoning* MLLMs do not carry over to *reasoning* models. We conduct ablation studies and comparative evaluations on *Ocean-R1* using VMCBench *dev set (1000 samples)*. For the comparative setting, we benchmark against prior contrastive-decoding and description-prior methods:

VCD [20] contrasts decoding distributions from the original image and a corrupted view; ICD [43] contrasts standard vs. disturbance-instruction decoding to subtract hallucinated concepts; AGLA [2] assembles global generation with prompt-relevant local cues via an augmented (masked) view; VDGD [11] grounds decoding with a self-generated visual description prefix to better support reasoning. The results are summarized in Fig. 6. Our findings are: **Finding 5: Performance trends align with expectations.** Based on Figure 6 (a–b), the accuracy trend over attention layers mirrors the CLUERECALL pattern in

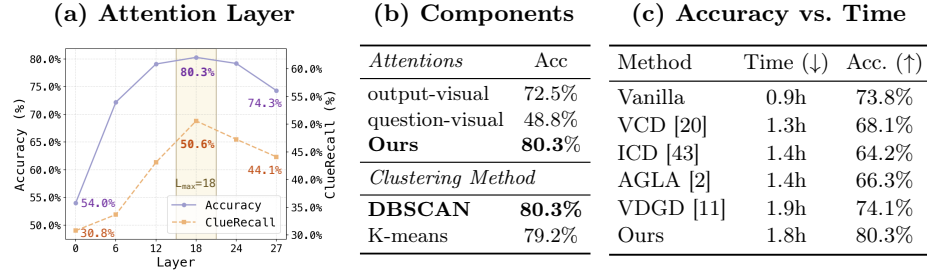


Fig. 6. Ablation Study and Comparative Evaluations. Default settings in the experiments are shown in **bold**. Additional ablations on hyperparameters (e.g., DBSCAN and z-score thresholds) are provided in the Appendix F [47].

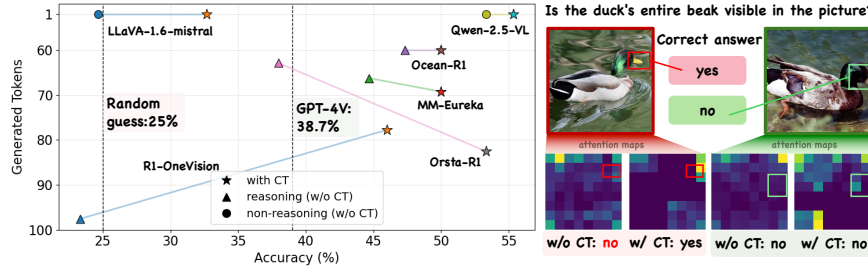


Fig. 7. Left: Accuracy versus output–token length on MMVP across models; **Right:** attention allocation with and without CLUETRACER.

Table 2. For **clustering**, DBSCAN is preferable to K-means, as it is less sensitive to noise and can naturally discard isolated noisy tokens when the attention map contains spurious activations; see Appendix C.3 [47] for a detailed discussion. **Finding 6: CLUETRACER outperforms prior inference-time baselines on reasoning models.** As shown in Fig. 6 (c), CLUETRACER consistently improves over baselines originally developed for non-reasoning settings, which are less effective under the long-context dynamics of reasoning models. In particular, contrastive-decoding methods can suffer from *bias accumulation* over long chains, causing decoding to drift and even reducing accuracy below the vanilla model, while description-prior approaches often fail to provide task-specific priors that are actually useful for solving the question.

6.5 Transfer CLUETRACER to Non-Reasoning MLLMs (RQ4)

To verify the transferability of CLUETRACER, we evaluate MMVP on *non-reasoning* MLLMs. Concretely, we adopt the *offline* setting: attention-guided crops produced by Ocean-R1 are fed to Qwen2.5-VL and LLaVA-1.6-Mistral. Results are summarized in Fig. 7. Our findings are:

Finding 7: ClueTracer broadly strengthens both reasoning and non-reasoning MLLMs. MMVP is designed to probe visual defects in multimodal models. As shown in Fig. 7, ClueTracer consistently improves performance; in particular, it moves several models—LLaVA-1.6, R1-OneVision, and ORSTA-R1—from near random guessing toward the GPT-4V level. In the qualitative examples of Fig. 7, without ClueTracer the models barely attend to the key region of the question, whereas with ClueTracer they shift focus to that region.

7 Conclusion

In this paper, we introduce ClueTracer, a new hallucination suppression approach for multimodal reasoning models that is training free, parameter free, and architecture agnostic, thus incurring minimal deployment cost. Concretely, ClueTracer leverages fourfold attention along the question→output→visual pathway to identify question relevant visual patches and steer focus toward task relevant regions, enabling more precise inference. Across both reasoning and non reasoning settings, ClueTracer yields an average improvement of **14.9** percentage points.

References

1. An, W., Nie, J., Tian, F., Lin, H., Wu, Y., Wang, Q., Zhang, X., Lu, S., et al.: Boosting knowledge utilization in multimodal large language models via adaptive logits fusion and attention reallocation. In: The Thirty-ninth Annual Conference on Neural Information Processing Systems (2025)
2. An, W., Tian, F., Leng, S., Nie, J., Lin, H., Wang, Q., Chen, P., Zhang, X., Lu, S.: Mitigating object hallucinations in large vision-language models with assembly of global and local attention. In: Proceedings of the Computer Vision and Pattern Recognition Conference. pp. 29915–29926 (2025)
3. Bai, S., Chen, K., Liu, X., Wang, J., Ge, W., Song, S., Dang, K., Wang, P., Wang, S., Tang, J., Zhong, H., Zhu, Y., Yang, M., Li, Z., Wan, J., Wang, P., Ding, W., Fu, Z., Xu, Y., Ye, J., Zhang, X., Xie, T., Cheng, Z., Zhang, H., Yang, Z., Xu, H., Lin, J.: Qwen2.5-vl technical report. arXiv preprint arXiv:2502.13923 (2025)
4. Bai, Z., Wang, P., Xiao, T., He, T., Han, Z., Zhang, Z., Shou, M.Z.: Hallucination of multimodal large language models: A survey. arXiv preprint arXiv:2404.18930 (2024)
5. Chen, S., Zhu, T., Zhou, R., Zhang, J., Gao, S., Niebles, J.C., Geva, M., He, J., Wu, J., Li, M.: Why is spatial reasoning hard for vlms? an attention mechanism perspective on focus areas. arXiv preprint arXiv:2503.01773 (2025)
6. Dong, B., Ni, M., Huang, Z., Yang, G., Zuo, W., Zhang, L.: Mirage: Assessing hallucination in multimodal reasoning chains of mllm. arXiv preprint arXiv:2505.24238 (2025)
7. Dong, Y., Liu, Z., Sun, H.L., Yang, J., Hu, W., Rao, Y., Liu, Z.: Insight-v: Exploring long-chain visual reasoning with multimodal large language models. In: Proceedings of the IEEE/CVF Conference on Computer Vision and Pattern Recognition (CVPR). pp. 9062–9072 (2025)

8. Duan, C., Fang, R., Wang, Y., Wang, K., Huang, L., Zeng, X., Li, H., Liu, X.: Got-r1: Unleashing reasoning capability of mllm for visual generation with reinforcement learning. In: arXiv preprint arXiv:2505.17022 (2025)
9. Ester, M., Kriegel, H., Sander, J., Xu, X.: A density-based algorithm for discovering clusters in large spatial databases with noise. In: Proceedings of the Second International Conference on Knowledge Discovery and Data Mining (KDD'96). pp. 226–231. AAAI Press, Portland, OR, USA (1996), <https://aaai.org/papers/kdd96-037-a-density-based-algorithm-for-discovering-clusters-in-large-spatial-databases-with-noise>
10. Fan, Y., He, X., Yang, D., Zheng, K., Kuo, C.C., Zheng, Y., Narayananaraju, S.J., Guan, X., Wang, X.E.: Grit: Teaching mllms to think with images. arXiv preprint arXiv:2505.15879 (2025)
11. Ghosh, S., Evuru, C.K.R., Kumar, S., Tyagi, U., Nieto, O., Jin, Z., Manocha, D.: Visual description grounding reduces hallucinations and boosts reasoning in lvlms. arXiv preprint arXiv:2405.15683 (2024)
12. Guan, T., Liu, F., Wu, X., Xian, R., Li, Z., Liu, X., Wang, X., Chen, L., Huang, F., Yacoob, Y., Manocha, D., Zhou, T.: Hallusionbench: An advanced diagnostic suite for entangled language hallucination and visual illusion in large vision-language models. In: Proceedings of the IEEE/CVF Conference on Computer Vision and Pattern Recognition (CVPR). pp. 14375–14385 (June 2024)
13. Guo, D., Yang, D., Zhang, H., Song, J., Wang, P., Zhu, Q., Xu, R., Zhang, R., Ma, S., Bi, X., Zhang, X., Yu, X., Wu, Y., Wu, Z.F., Gou, Z., Shao, Z., Li, Z., Gao, Z., Liu, A., Xue, B., Wang, B., Wu, B., Feng, B., Lu, C., Zhao, C., Deng, C., Ruan, C., Dai, D., Chen, D., Ji, D., Li, E., Lin, F., Dai, F., Luo, F., Hao, G., Chen, G., Li, G., Zhang, H., Xu, H., Ding, H., Gao, H., Qu, H., Li, H., Guo, J., Li, J., Chen, J., Yuan, J., Tu, J., Qiu, J., Li, J., Cai, J.L., Ni, J., Liang, J., Chen, J., Dong, K., Hu, K., You, K., Gao, K., Guan, K., Huang, K., Yu, K., Wang, L., Zhang, L., Zhao, L., Wang, L., Zhang, L., Xu, L., Xia, L., Zhang, M., Zhang, M., Tang, M., Zhou, M., Li, M., Wang, M., Li, M., Tian, N., Huang, P., Zhang, P., Wang, Q., Chen, Q., Du, Q., Ge, R., Zhang, R., Pan, R., Wang, R., Chen, R.J., Jin, R.L., Chen, R., Lu, S., Zhou, S., Chen, S., Ye, S., Wang, S., Yu, S., Zhou, S., Pan, S., Li, S.S., Zhou, S., Wu, S., Yun, T., Pei, T., Sun, T., Wang, T., Zeng, W., Liu, W., Liang, W., Gao, W., Yu, W., Zhang, W., Xiao, W.L., An, W., Liu, X., Wang, X., Chen, X., Nie, X., Cheng, X., Liu, X., Xie, X., Liu, X., Yang, X., Li, X., Su, X., Lin, X., Li, X.Q., Jin, X., Shen, X., Chen, X., Sun, X., Wang, X., Song, X., Zhou, X., Wang, X., Shan, X., Li, Y.K., Wang, Y.Q., Wei, Y.X., Zhang, Y., Xu, Y., Li, Y., Zhao, Y., Sun, Y., Wang, Y., Yu, Y., Zhang, Y., Shi, Y., Xiong, Y., He, Y., Piao, Y., Wang, Y., Tan, Y., Ma, Y., Liu, Y., Guo, Y., Ou, Y., Wang, Y., Gong, Y., Zou, Y., He, Y., Xiong, Y., Luo, Y., You, Y., Liu, Y., Zhou, Y., Zhu, Y.X., Huang, Y., Li, Y., Zheng, Y., Zhu, Y., Ma, Y., Tang, Y., Zha, Y., Yan, Y., Ren, Z.Z., Ren, Z., Sha, Z., Fu, Z., Xu, Z., Xie, Z., Zhang, Z., Hao, Z., Ma, Z., Yan, Z., Wu, Z., Gu, Z., Zhu, Z., Liu, Z., Li, Z., Xie, Z., Song, Z., Pan, Z., Huang, Z., Xu, Z., Zhang, Z., Zhang, Z.: DeepSeek-R1 incentivizes reasoning in LLMs through reinforcement learning. Nature **645**(8081), 633–638 (Sep 2025). <https://doi.org/10.1038/s41586-025-09422-z>, <https://doi.org/10.1038/s41586-025-09422-z>
14. He, K., Gkioxari, G., Dollár, P., Girshick, R.: Mask r-cnn. In: Proceedings of the IEEE international conference on computer vision. pp. 2961–2969 (2017)
15. Huang, W., Jia, B., Zhai, Z., Cao, S., Ye, Z., Zhao, F., Xu, Z., Hu, Y., Lin, S.: Vision-r1: Incentivizing reasoning capability in multimodal large language models. arXiv preprint arXiv:2503.06749 (2025)

16. Im, E.W., Ali, M.K., Gupta, V.: Self-augmented visual contrastive decoding. arXiv preprint arXiv:2510.13315 (2025)
17. Jiang, C., Heng, Y., Ye, W., Yang, H., Xu, H., Yan, M., Zhang, J., Huang, F., Zhang, S.: Vlm- r^3 : Region recognition, reasoning, and refinement for enhanced multimodal chain-of-thought. arXiv preprint arXiv:2505.16192 (2025)
18. Kang, S., Kim, J., Kim, J., Hwang, S.J.: See what you are told: Visual attention sink in large multimodal models. arXiv preprint arXiv:2503.03321 (2025)
19. Kim, J., Kim, H., Yeonju, K., Ro, Y.M.: Code: Contrasting self-generated description to combat hallucination in large multi-modal models. Advances in Neural Information Processing Systems **37**, 133571–133599 (2024)
20. Leng, S., Zhang, H., Chen, G., Li, X., Lu, S., Miao, C., Bing, L.: Mitigating object hallucinations in large vision-language models through visual contrastive decoding. In: Proceedings of the IEEE/CVF Conference on Computer Vision and Pattern Recognition. pp. 13872–13882 (2024)
21. Li, Y., Du, Y., Zhou, K., Wang, J., Zhao, X., Wen, J.R.: Evaluating object hallucination in large vision-language models. In: Proceedings of the 2023 Conference on Empirical Methods in Natural Language Processing. pp. 292–305. Association for Computational Linguistics, Singapore (December 2023). <https://doi.org/10.18653/v1/2023.emnlp-main.20>, <https://aclanthology.org/2023.emnlp-main.20/>
22. Li, Z., Shi, H., Gao, Y., Liu, D., Wang, Z., Chen, Y., Liu, T., Zhao, L., Wang, H., Metaxas, D.N.: The hidden life of tokens: Reducing hallucination of large vision-language models via visual information steering. arXiv preprint arXiv:2502.03628 (2025)
23. Lin, T., Maire, M., Belongie, S., Bourdev, L., Girshick, R., Hays, J., Perona, P., Ramanan, D., Dollár, P., Zitnick, C.L.: Microsoft coco: Common objects in context. In: Fleet, D.J., Pajdla, T., Schiele, B., Tuytelaars, T. (eds.) Computer Vision – ECCV 2014. Lecture Notes in Computer Science, vol. 8693, pp. 740–755. Springer, Cham (2014). https://doi.org/10.1007/978-3-319-10602-1_48, https://doi.org/10.1007/978-3-319-10602-1_48
24. Liu, C., Xu, Z., Wei, Q., Wu, J., Zou, J., Wang, X.E., Zhou, Y., Liu, S.: More thinking, less seeing? assessing amplified hallucination in multimodal reasoning models. arXiv preprint arXiv:2505.21523 (2025)
25. Liu, H., Li, C., Li, Y., Li, B., Zhang, Y., Shen, S., Lee, Y.J.: Llava-next: Improved reasoning, ocr, and world knowledge (January 2024), <https://llava-vl.github.io/blog/2024-01-30-llava-next/>
26. Liu, H., Li, C., Wu, Q., Lee, Y.J.: Visual instruction tuning (2023)
27. Liu, H., Li, C., Wu, Q., Lee, Y.J.: Visual instruction tuning. arXiv preprint arXiv:2304.08485 (2023), <https://arxiv.org/abs/2304.08485>
28. Liu, Y., Peng, B., Zhong, Z., Yue, Z., Lu, F., Yu, B., Jia, J.: Seg-zero: Reasoning-chain guided segmentation via cognitive reinforcement. In: arXiv preprint arXiv:2503.06520 (2025)
29. Lu, H., Liu, Y., Xu, J., Nan, G., Yu, Y., Chen, Z., Wang, K.: Auditing meta-cognitive hallucinations in reasoning large language models. arXiv preprint arXiv:2505.13143 (2025)
30. Lu, P., Mishra, S., Xia, T., Qiu, L., Chang, K.W., Zhu, S.C., Tafjord, O., Clark, P., Kalyan, A.: Learn to explain: Multimodal reasoning via thought chains for science question answering. arXiv preprint arXiv:2209.09513 (2022)
31. Ma, Y., Du, L., Shen, X., Chen, S., Li, P., Ren, Q., Ma, L., Dai, Y., Liu, P., Yan, J.: One rl to see them all: Visual triple unified reinforcement learning. arXiv preprint arXiv:2505.18129 (2025)

32. Meng, F., Du, L., Liu, Z., Zhou, Z., Lu, Q., Fu, D., Shi, B., Wang, W., He, J., Zhang, K., Luo, P., Qiao, Y., Zhang, Q., Shao, W.: Mm-eureka: Exploring visual aha moment with rule-based large-scale reinforcement learning (2025), <https://arxiv.org/abs/2503.07365>
33. Ming, L., Li, Y., Chen, S., Xu, J., Zhou, Z., Chen, W.: Ocean-r1: An open and generalizable large vision-language model enhanced by reinforcement learning. <https://github.com/VLM-RL/Ocean-R1> (2025), accessed: 2025-04-03
34. Tan, H., Ji, Y., Hao, X., Lin, M., Wang, P., Wang, Z., Zhang, S.: Reason-rft: Reinforcement fine-tuning for visual reasoning. In: arXiv preprint arXiv:2503.20752 (2025)
35. Thawakar, O., Dissanayake, D., More, K., Thawkar, R., Heakl, A., Ahsan, N., Li, Y., Zumri, M., Lahoud, J., Anwer, R.M., et al.: Llamav-01: Rethinking step-by-step visual reasoning in llms. arXiv preprint arXiv:2501.06186 (2025)
36. Tong, S., Liu, Z., Zhai, Y., Ma, Y., LeCun, Y., Xie, S.: Eyes wide shut? exploring the visual shortcomings of multimodal llms (2024). <https://doi.org/10.48550/arXiv.2401.06209>, <https://arxiv.org/abs/2401.06209>
37. Tu, C., Ye, P., Zhou, D., Bai, L., Yu, G., Chen, T., Ouyang, W.: Attention reallocation: Towards zero-cost and controllable hallucination mitigation of mllms. International Journal of Computer Vision **134**(1), 22 (2026)
38. Vaswani, A., Shazeer, N., Parmar, N., Uszkoreit, J., Jones, L., Gomez, A.N., Kaiser, Ł., Polosukhin, I.: Attention is all you need. In: Advances in Neural Information Processing Systems. pp. 5998–6008 (2017)
39. Walpole, R.E., Myers, R.H., Myers, S.L., Ye, K.: Probability and Statistics for Engineers and Scientists. Pearson, 9th edn. (2011)
40. Wang, J., Lin, K.Q., Cheng, J., Shou, M.Z.: Think or not? selective reasoning via reinforcement learning for vision-language models. arXiv preprint arXiv:2505.16854 (2025)
41. Wang, K., Pan, J., Shi, W., Lu, Z., Zhan, M., Li, H.: Measuring multimodal mathematical reasoning with MATH-Vision dataset. arXiv preprint arXiv:2402.14804 (2024)
42. Wang, W., Gao, Z., Chen, L., Chen, Z., Zhu, J., Zhao, X., Liu, Y., Cao, Y., Ye, S., Zhu, X., Lu, L., Duan, H., Qiao, Y., Dai, J., Wang, W.: Visualprm: An effective process reward model for multimodal reasoning. In: arXiv preprint arXiv:2503.10291 (2025)
43. Wang, X., Pan, J., Ding, L., Biemann, C.: Mitigating hallucinations in large vision-language models with instruction contrastive decoding. arXiv preprint arXiv:2403.18715 (2024)
44. Wang, X., Yang, Z., Feng, C., Lu, H., Li, L., Lin, C., Lin, K., Huang, F., Wang, L.: Sota with less: Mcts-guided sample selection for data-efficient visual reasoning self-improvement. In: arXiv preprint arXiv:2504.07934 (2025)
45. Wang, Y., Wu, S., Zhang, Y., Yan, S., Liu, Z., Luo, J., Fei, H.: Multimodal chain-of-thought reasoning: A comprehensive survey. arXiv preprint arXiv:2503.12605 (2025)
46. Wu, J., Shi, Z., Wang, S., Huang, J., Yin, D., Yan, L., Cao, M., Zhang, M.: Mitigating hallucinations in large vision-language models via entity-centric multimodal preference optimization. arXiv preprint arXiv:2506.04039 (2025)
47. Xi, G.: CLUETRACER appendix (2026), supplemental material (appendix-clue-tracer.pdf) will be uploaded soon
48. Xu, H., Wu, X., Wang, W., Li, Z., Zheng, D., Chen, B., Hu, Y., Kang, S., Ji, J., Zhang, Y., et al.: Redstar: Does scaling long-cot data unlock better slow-reasoning systems? arXiv preprint arXiv:2501.11284 (2025)

49. Yang, Y., He, X., Pan, H., Jiang, X., Deng, Y., Yang, X., Lu, H., Yin, D., Rao, F., Zhu, M., Zhang, B., Chen, W.: R1-onevision: Advancing generalized multimodal reasoning through cross-modal formalization (2025). <https://doi.org/10.48550/arXiv.2503.10615>, <https://arxiv.org/abs/2503.10615>
50. Yao, H., Huang, J., Wu, W., Zhang, J., Wang, Y., Liu, S., Wang, Y., Song, Y., Feng, H., Shen, L., Tao, D.: Mulberry: Empowering vision-language models with o1-like reasoning and reflection via collective monte carlo tree search. arXiv preprint arXiv:2412.18319 (2024)
51. Ye, Z., Li, Q., Feng, X., Qin, L., Huang, Y., Li, B., Jiang, K., Xiang, Y., Zhang, Z., Lu, Y., et al.: Claim: Mitigating multilingual object hallucination in large vision-language models with cross-lingual attention intervention. arXiv preprint arXiv:2506.11073 (2025)
52. Yi, S., Shang, L.: Corgi: Verified chain-of-thought reasoning with visual grounding. arXiv preprint arXiv:2508.00378 (2025)
53. Yu, T., Yao, Y., Zhang, H., He, T., Han, Y., Cui, G., Hu, J., Liu, Z., Zheng, H.T., Sun, M., et al.: Rlhf-v: Towards trustworthy mllms via behavior alignment from fine-grained correctional human feedback. In: Proceedings of the IEEE/CVF Conference on Computer Vision and Pattern Recognition. pp. 13807–13816 (2024)
54. Zhang, D., Wu, J., Lei, J., Che, T., Li, J., Xie, T., Huang, X., Zhang, S., Pavone, M., Li, Y., et al.: Llama-berry: Pairwise optimization for o1-like olympiad-level mathematical reasoning. arXiv preprint arXiv:2410.02884 (2024)
55. Zhang, H., Liu, Z., Zhao, Y., Zheng, J., Zhuang, C., Gu, J., Chen, G.: Fast chain-of-thought: A glimpse of future from jacobi decoding leads to answers faster. In: arXiv preprint arXiv:2311.08263 (2024)
56. Zhang, J., Huang, J., Yao, H., Liu, S., Zhang, X., Lu, S., Tao, D.: R1-vl: Learning to reason with multimodal large language models via step-wise group relative policy optimization. In: arXiv preprint arXiv:2503.12937 (2025)
57. Zhang, R., Zhang, B., Li, Y., Zhang, H., Sun, Z., Gan, Z., Yang, Y., Pang, R., Yang, Y.: Improve vision language model chain-of-thought reasoning. arXiv preprint arXiv:2410.16198 (2024)
58. Zhang, X., Gao, Z., Zhang, B., Li, P., Zhang, X., Liu, Y., Yuan, T., Wu, Y., Jia, Y., Zhu, S.C., et al.: Chain-of-focus: Adaptive visual search and zooming for multimodal reasoning via rl. arXiv preprint arXiv:2505.15436 (2025)
59. Zhang, Y., Su, Y., Liu, Y., Wang, X., Burgess, J., Sui, E., Wang, C., Aklilu, J., Lozano, A., Wei, A., Schmidt, L., Yeung-Levy, S.: Automated generation of challenging multiple-choice questions for vision language model evaluation. In: Proceedings of the IEEE/CVF Conference on Computer Vision and Pattern Recognition (CVPR). pp. 29580–29590 (June 2025)
60. Zhang, Z., Zhang, A., Li, M., Zhao, H., Karypis, G., Smola, A.: Multimodal chain-of-thought reasoning in language models. arXiv preprint arXiv:2302.00923 (2023), <https://arxiv.org/abs/2302.00923>
61. Zhao, Y., Yin, H., Zeng, B., Wang, H., Shi, T., Lyu, C., Wang, L., Luo, W., Zhang, K.: Marco-o1: Towards open reasoning models for open-ended solutions. arXiv preprint arXiv:2411.14405 (2024)
62. Zheng, G., Qian, J., Tang, J., Yang, S.: Why lvlms are more prone to hallucinations in longer responses: The role of context. In: Proceedings of the IEEE/CVF International Conference on Computer Vision. pp. 4101–4113 (2025)
63. Zhou, G., Yan, Y., Zou, X., Wang, K., Liu, A., Hu, X.: Mitigating modality prior-induced hallucinations in multimodal large language models via deciphering attention causality. arXiv preprint arXiv:2410.04780 (2024)

64. Zou, X., Wang, Y., Yan, Y., Lyu, Y., Zheng, K., Huang, S., Chen, J., Jiang, P., Liu, J., Tang, C., et al.: Look twice before you answer: Memory-space visual retracing for hallucination mitigation in multimodal large language models. arXiv preprint arXiv:2410.03577 (2024)